



Rheology assessment and barite sag in a typical North Sea oil-based drilling fluid at HPHT conditions

Titus Ntow Ofei¹ · Elie Ngouamba¹ · Nils Opedal¹ · Bjørnar Lund¹ · Arild Saasen²

Received: 29 April 2022 / Revised: 2 March 2023 / Accepted: 5 March 2023 / Published online: 21 March 2023
© The Author(s) 2023

Abstract

The occurrence of barite sag in drilling fluids has relatively often been the cause for gas kicks in oilwell drilling. The subsequent absorption of gas into drilling fluid could lower the density and reduce the viscosity of the drilling fluid, thereby aggravating both pressure control and hole cleaning. In this paper, we present experimental measurements of rheological properties and barite sag in a typical North Sea oil-based drilling fluid at downhole pressure and temperature conditions. A new experimental apparatus was setup for barite sag measurements at static condition with operational temperature and pressure capabilities up to 200 °C (392 °F) and 1000 bar (14,503.8 psi), respectively. Rheometry measurements were conducted on fluid samples with and without barite particles at operating conditions up to 90 °C and 100 bar. We observed that at a typical shear rate of 250 s⁻¹, which is experienced in 8.5" hole annulus, the viscosity of fluid sample with barite increased nearly three times as that of the fluid sample without barite as the temperature and pressure increased. However, temperature effect on viscosity dominates at high shear rates compared to pressure effect. Furthermore, the fluid samples showed more shear-thinning effect with increasing yield stress as the temperature increased. On the other hand, barite sag measurements revealed that whereas fluid samples under high pressure are less prone to sag, high temperature fluid samples, however, promote sag significantly. The data from this study are useful to validate extrapolations used in computational models and to improve understanding and operational safety of sag phenomena at downhole conditions. We also discuss the importance of this study in optimizing drilling operations.

Keywords Barite sag · Oil-based drilling fluid · HPHT · Rheology · Viscoelasticity · Herschel–Bulkley model

1 Introduction

Drilling fluid can be water or oil-based and is densified by the addition of solid weight materials, most commonly barite. Drilling fluids serve many functions like transporting drilled cuttings to the surface, maintaining pressure control at the bottom hole, preventing damage to the formation or unwanted formation fluid influx. In many instances, the stability of the drilling fluid is influenced by several factors, including the rheological properties of the fluid, particle density, shape, size, concentration, and structural strength of the network [41]. The tendency of suspended weight

materials to settle in drilling fluid is termed sag and can lead to variation in fluid density. If this variation is not controlled, it can lead to pressure-control-related issues like gas kicks or blow outs, fluctuation in torque and drag loads, difficulty in running of casing, displacement inefficiency during cementing operation, lost circulation, stuck pipe, among others [41, 47, 48, 51]. Suspended weight material particles in drilling fluids in inclined wellbores tend to settle much more as a result of creating dynamic conditions by the sag itself, which may accelerate the sag process in a phenomenon called Boycott settling [12, 26]. Other effects accelerating sag include low to moderate pumping rate, disturbances from tripping drill pipe or logging tools, or slow drill pipe rotation speed. As a result, sag in field operations can be more severe than in static condition [15, 27, 28, 47].

Gas kicks have often been caused by barite sag in the wellbore. Then, a gas kick can in turn accelerate the sag because the gas can thin out the base fluid. Among the two main types of drilling fluids, water-based drilling fluids are

✉ Titus Ntow Ofei
ofeititus@gmail.com

¹ SINTEF, Trondheim, Norway

² Department of Energy and Petroleum Technology, University of Stavanger, Stavanger, Norway

known to be less prone to sag than oil-based drilling fluids. Industry rules of thumb exist to minimize barite sag in field operations. It is often required to dilute or add to the drilling fluid with no more than 5% premix per circulation with a pressure loss of 50 bar across the drill bit when drilling with oil-based drilling fluids [33]. Thus, adjusting the viscosity profile during a drilling operation can be a time-consuming process. At downhole conditions of high temperature and pressure, oil-based drilling fluids are preferred due to their stable viscosity profile, higher thermal tolerance, and better shale inhibition properties compared to water-based drilling fluids [3, 9].

There are several measurement techniques available in the literature for analyzing barite sag in drilling fluids. These include the static test cell, standard viscometers, and lab-scale flow loops among others [33, 37]. More advanced methods using rotational rheometers have also been tested [4, 16, 29, 44]. Whereas most authors have attempted to correlate sag to rheological data [24, 30, 31, 39, 48], others also investigated the relationship between drilling operating parameters and sag [21, 28, 35, 41, 47].

Drilling fluids are commonly formulated and analyzed according to the American Petroleum Institute (API) standards and at elevated temperatures [31]. A few studies have investigated the effect of elevated downhole temperature or pressure on the rheological properties and barite sag in drilling fluids. [22] examined the sag rate in three field invert emulsion drilling fluids in a dynamic sag tester under temperature and pressure conditions of 160 °C (320°F) and 137.9 bar (2000 psi), respectively. The dynamic sag tester consists of a tube which is set at 45° inclination. A rotating shaft is mounted inside the tube which shears the testing fluid. The tube can be pressurized and heated at the same time. As the particulates in the fluid sample start settling, the center of mass of the inclined tube changes. The force required to maintain the tube in equilibrium position is measured in terms of electrical signal, voltage. This voltage is finally converted into the rate of particulate settling. Other authors conducted their sag and rheology studies on oil-based drilling fluids considering only different temperature conditions [17].

At high temperature and pressure conditions, limited data are reported in literature on the rheological behavior of drilling fluids, and computations are often based on extrapolating from existing models beyond their validated range, which gives unreliable results [5]. Oil-based drilling fluids properties including saturation pressure, density and viscosity were analyzed at high temperature and pressure conditions up to 315.6 °C (600°F) and 1723.7 bar (25,000 psi), respectively [3, 49]. Wang et al. [50] conducted static sag and rheological measurements at different pressures and temperatures at HPHT conditions. Rheological measurements were conducted using a 6-speed viscometer and particle carrying

capacity was assessed in terms of a YP from the 600 and 300 RPM measurement values. Measurement at HPHT conditions of a yield stress value which is more representative for low shear rate and static situations is technically challenging.

Analysis of the combination of rheological properties and sag in oil-based drilling fluid under extreme downhole temperature and pressure conditions have not yet received much attention in the open literature. In this study, we produced measurements of rheological properties and barite sag in a typical oil-based drilling fluid with composition applicable to North Sea applications at high pressure and high temperature conditions. This could provide the basis for validation of existing models and thus contribute toward filling the knowledge gap related to high pressure and high temperature conditions.

2 Materials and methods

2.1 Fluid components and compositions

Two batches (batch 1 and batch 2) of drilling fluids were formulated with the same composition with barite particles. Their differences are that, the refined mineral oil used in batch 1 is EDC 95/11 with a density of 814 kg m⁻³ and a viscosity of 4.8 mPa s, while batch 2 was formulated with ESCAID 120 ULA refined mineral oil with density of 820 kg m⁻³ and a viscosity of 1.89 mPa s. In both batches, we formulated common oil-based drilling fluids (OBDF) with density of 1430 kg m⁻³ (SG = 1.43), oil/water ratio (OWR) of 80/20 and composition which is representative for North Sea operations. In addition, a separate batch 2B was formulated without barite particles maintaining OWR of 80/20 and the fluid density was recorded as 966 kg m⁻³. The water phase was a premixed brine to ensure proper dissolution of the salt. The various components of the oil-based drilling fluids with and without barite particles including their compositions and mixing time are shown in Table 1.

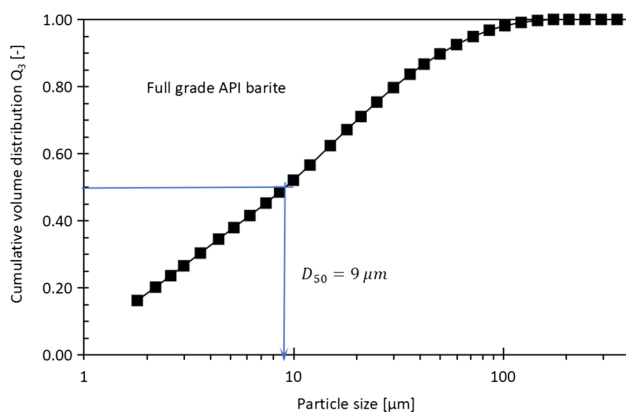
2.2 Particle size distribution

The selected barite was procured to follow the specifications from the American Petroleum Institute [6]. Hence, the density should be 4.20 sg and the amount of water-soluble alkaline earth materials should be less than 250 mg/kg. The particle size residue larger than 75 µm should be less than 3% and the particle fraction less than 6 µm should be less than 30%. Recently, it has been known that the density seldom exceeds 4.15 sg [2]. The effect of such a small difference in density is assumed to be insignificant, and no effort was used to determine this more accurately.

To characterize the particle size distribution in detail of the procured API barite, the light scattering (LS) particle

Table 1 Components of 1 L oil-based drilling fluid (OBDF)

Mixing order	Product	S.G = 1.43 (OWR = 80/20) Batch 1 and 2 Concentration (g/L)	S.G = 0.966 (OWR = 80/20) Batch 2B w/o barite Concentration (g/L)	Mixing time (min.)
1	Refined mineral oil (base fluid)	501.0	588.6	–
2	Emulsifier	20.0	23.5	2
3	Viscosifier (organophilic clays)	22.0	27.0	8
4	Lime	20.0	23.5	5
5	Fluid loss agent	10.0	10.6	5
6	Calcium chloride brine	199.0	234.4	15
7	API barite (weight material)	610.0	0.0	–
8	Calcium carbonate (simulated low gravity solids)	50.0	58.6	10

**Fig. 1** Particle size distribution of the applied full grade API barite

size analyzer was used. This instrument can detect particle sizes ranging from 0.04 to 2000 μm using light diffraction mechanism powered by a laser light with a wavelength of 750 nm. A beam of light is formed as the laser radiation is passed through a spatial filter. As the beam of light passes through the sample cell, the light is scattered by particles which are suspended in the medium (liquid or gas). The scattering pattern (intensity of transmitted and back-scattered light) depends on both the particle size and the volume fraction of particles (Coulter LS series, 2011). Figure 1 shows the measured particle size distribution (PSD) of a dry sample of full grade API barite, showing a D_{50} value of 9.0 μm . The value of D_x represents the $x\%$ of the particles by volume having diameter smaller than this value.

The water phase droplet sizes in oil-based drilling fluids are in a range from around 1 μm , observed in a well sheared fluid sample, to several microns dependent on the shear history of the fluids [25, 32]. With an oil/water ratio of 80/20 or less the interdroplet distance is in magnitude of the droplet size or, for lower oil/water ratios, less than the droplet size. In the absence of flow, or with only a very small shear rate,

Brownian motion will maintain a sort of crystalline droplet position structure in average as described by Ackerson [1]. As long as this crystalline structure exists, a resistance to flow like a yield stress will be observed. If the formation of this crystalline structure is prevented, like in the presence of vibrations, the yield stress will be strongly reduced or disappear [40]. At the same time, a linear viscoelastic range can be measured as long as the frequency and amplitude are small enough for the crystalline droplet position placement to be formed. At a strain large enough such that droplets must start to leapfrog to maintain the strain, the yield stress slowly is broken, and the dynamic viscosity measurements are no longer in the linear viscoelastic range. Hence, the stress at the end of the linear viscoelastic range can be understood as the static yield stress. When all the droplets are positioned in a seemingly random position in average, the G'' value will overtake the G' value and the effect of the Brownian motion will no longer be of significance. The stress at this point is often referred to as the dynamic yield stress since it is the shear stress where the time-dependent formation of the yield stress starts on a ramp down curve in a shear stress versus shear rate curve. If more rheological details are needed when the stress is around the yield stress, it is also possible to treat such a fluid as a wet powder and try to predict the yield stress from Mohr–Coloumb law [34]. However, this approach has not been followed in the present article.

For most commercial barite made in accordance with API, the D_{50} value will typically be in the range 10 to 25 μm . D_{50} values outside this range are still also common. The maximum particle size is usually around 75 μm . Therefore, the finer shaker screens used in primary solids control are often set at 200 mesh to allow particles less than 75 μm through and thereby not losing any of the added barite particles. By definition, half of the barite volume is larger than the D_{50} value. These larger particles are found to be vulnerable for sagging. The motion will set up flow that depends

strongly on the microstructure of the yield stress, and, hence, on both the static and dynamic yield stresses as measured using dynamic viscosity measurements.

2.3 Fluid mixing procedure

In preparation of batch 1 and batch 2, we followed the exact same mixing procedure as described in [29]. Whereas batch 1 was mixed with a Hamilton Beach mixer at 6000 rpm, batches 2 and 2B were mixed with an OFITE mixer at 6000 rpm. The mixing procedure is summarized in the following paragraph. It should be noted that all the components of the drilling fluid including the formulation procedure were provided by the drilling fluid supplier.

The temperature of the fluid sample was monitored not to exceed 65 °C during the mixing process. If the fluid sample reaches 65 °C, the mixing cup was placed in a water bath during further mixing to cool it down. The base oil and emulsifier were added to the mixing container and mixed for 2 min at a speed adequate to create a vortex. The organophilic clay viscosifiers were slowly added into the vortex and mixed for 8 min, ensuring that all have completely dispersed and that none adhered to the side of the mixing container. Afterward, the lime was added slowly into the vortex and mixed for 5 min. The fluid loss additive was then added slowly into the vortex and also mixed for 5 min, ensuring that all have completely dispersed and that none adhered to the side of the mixing container. The required quantity of prepared brine was added and mixed for a total of 5 min. The weighting agent barite was added during a 5-min period and mixed for further 20 min. Finally, the fluid loss material was added and mixed for 10 min, ensuring that all additives were completely dispersed and that none adhered to the side of the mixing container.

We measured the density of the fluid samples using Anton Paar DMA 5000 instrument at atmospheric condition. The emulsion stability (ES) of the fluid samples of batch 1 was tested using an ES meter (emulsion stability tester). This instrument applies a precision voltage-ramped sinusoidal signal across a pair of parallel flat plate electrodes to read the voltage, usually in a range from 0 to 2000 V, across the parallel plate. The ES test indicates the emulsion and oil-wetting qualities of the fluid sample. A stable fluid sample will have a high voltage reading, before the fluid becomes conducting. To measure the concentration of hydrogen ions in the fluid sample, a pH meter was used. The recorded ES and pH values of the batch 1 fluid sample are 922 V and 10.4 respectively, at atmospheric pressure and temperature. Although a high ES value is not necessarily proof of a stable emulsion, we note that this value is similar to that measured by Borges et al. [11] for an oil-based drilling fluid with a similar OWR.

2.4 Rheological characterization

The rheological measurements were carried out under three conditions: (1) atmospheric pressure and temperature, (2) elevated temperature (90 °C) at atmospheric pressure, and (3) elevated pressure and temperature (90 °C and 100 bar). A scientific rheometer (Anton Paar MCR102) was used with two different geometries. The default geometry was a grooved bob (CC27/P6-SN28482) and a smooth measuring cup. Some measurements and in particular all measurements at 100 bar were conducted with a pressure cell assembly (CC25/Pr150/In/A1/SS). This consists of a magnetic coupling, pressure head, a grooved flat-bottom measuring bob (CC33.2-0-62/PR/P6-SN88732). The pressure cell assembly has a maximum capacity of 150 bar and 180 °C and was controlled by two syringe pumps. In this rheometry experiment using the pressure cell, the fluid sample was transferred from a sample cylinder via a pressurizing unit (pump) which enters the bottom of the pressure cell through a 2.4 m long 1/8" tubing section with several high-pressure valves. The pumps thereby function as a pressurizing unit for the rheometer. Unless stated otherwise, the results presented were conducted using the default measurement system.

The flow curves which show the relationship between the shear stress versus the shear rate were measured under a controlled shear rate. The fluid sample was pre-sheared at a constant shear rate of 1000 s⁻¹ for 300 s to uniformly disperse the barite particles within the sample. Immediately after that, the shear rate was ramped down linearly from 1000 to 1.0 s⁻¹ for 100 measuring points with a 5 s measuring duration per point. To capture the flow characteristics in the low shear rate region, the shear rate was ramped down logarithmically from 1.0 to 0.01 s⁻¹ for 40 measuring points with each point duration of 4 s. The ramp down was followed by a ramp up sequence following the same protocol, to capture the difference between the two flow curves. It is reported in the literature that differences between the ramp down and ramp up flow curves indicate the occurrence of thixotropy of the fluid sample [13, 20]. From this experiment, we observed an insignificant difference between the ramp down and ramp up flow curves.

2.5 Experimental setup for barite sag test cell at HPHT conditions

The experimental setup used to measure the barite sag at downhole pressure and temperature conditions is described by Flatabø et al. [18]. The setup uses stainless steel piston cylinders with operating pressure up to 1000 bar and a temperature range from 20 to 200 °C. The piston cylinders serve as mixing and waste cylinders and are controlled by two syringe pumps operating in dual mode. Paraffin oil is used to pressurize the pump and cylinder pistons.

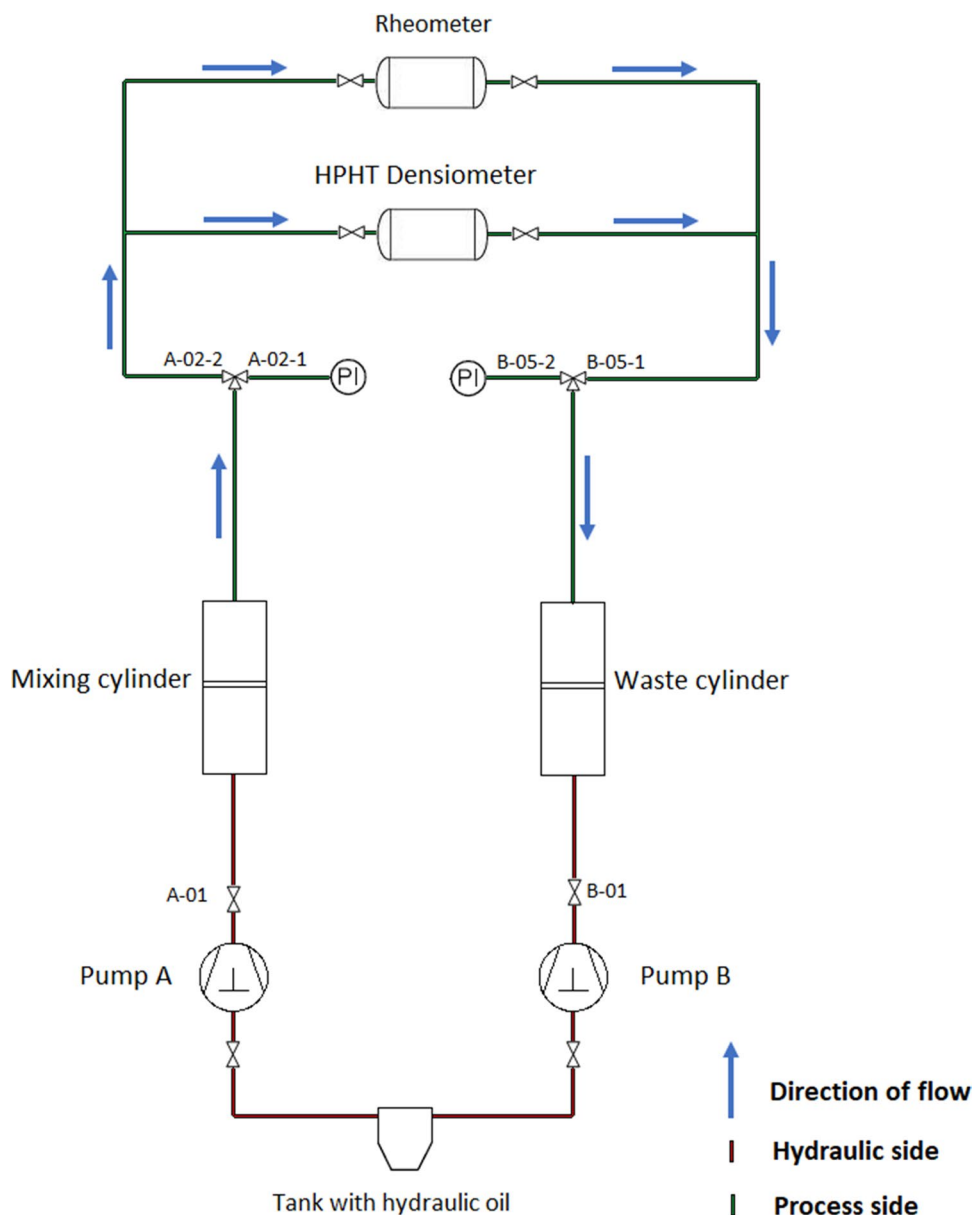
The mixing cylinder which contains the fluid sample is encased in a heating jacket with the capacity of heating up to 200 °C, which controls the temperature in the cylinder. The mixing cylinder is mounted on a rocking mechanism to enhance temperature equilibration of the test fluid and also to improve particle suspension. Another equipment as part of the setup is the Anton Paar DMA HPM HPHT (high pressure and high temperature) density measuring cell (also known as densitometer) along with an mPDS 5 CPU control unit. The setup is also fitted with two pressure transducers for measuring the pressure produced by the pumps as the fluid sample flows from the mixing cylinder into the DMA HPM density meter and backpressure in the waste cylinder. In this study, a 450 mL of the drilling fluid was filled into the mixing cylinder. The experiments were

conducted for a temperature range from 50 to 200 °C and pressure range from 100 to 800 bar. Figure 2 shows the sketch of the experimental setup for measuring barite sag at HPHT condition.

The following working procedure was adopted for the measurement of barite sag at HPHT condition.

- a. The pump piston (A) in the mixing cylinder was adjusted to the required fluid volume. The mixing cylinder was filled with a 450 mL drilling fluid and the air in the tubing was bled off.
- b. The mixing cylinder was heated using the heating jacket to the desired temperature and pressure in the mixing cylinder was adjusted to the desired pressure using the pump piston (A).

Fig. 2 Simplified sketch of experimental setup showing all process components



- c. The motor connecting the mixing cylinder was activated for 120 min to rock the cylinder to enhance temperature equilibration of the fluid sample and to improve particle suspension in the fluid sample.
- d. The DMA HPM density measuring cell was placed into a heating chamber and heated up to the same temperature as in the mixing cylinder.
- e. The fluid sample was flushed into the DMA HPM density measuring cell and bypassed into the backpressure piston cylinder to measure the initial density.
- f. To maintain the pressure in the density measuring cell, the pressure in the backpressure cylinder was adjusted to be equal to the pressure in the mixing cylinder using the pump piston (B).
- g. The mixing cylinder was positioned vertically and the fluid system was allowed to remain static for 24 h at the specified pressure and temperature to promote particle sedimentation within the cylinder.
- h. Afterward, the drilling fluid was bled into the DMA HPM density measuring cell and bypassed into the backpressure piston cylinder to measure the final density while maintaining the backpressure.

When bleeding in this volume, we first measured the top fluid being of free oil. Thereafter, we measured the top suspension fluid density ρ_{final} , and the bulk fluid density ρ_{initial} . The top suspension and bulk fluid densities are used in the sag factor equation

$$\text{Sag factor (SF)} = \frac{\rho_{\text{initial}}}{\rho_{\text{initial}} + \rho_{\text{final}}}. \quad (1)$$

For a fluid to exhibit perfect particle suspension characteristics, the sag factor should be 0.50, while a sag factor greater than 0.53 is considered to give inadequate suspension properties, hence, the fluid sample is prone to sag [23, 24]. In Table 2, we describe the functions of the physical components of the experimental setup.

The HPHT barite sag test cell was pressure-tested and calibrated using paraffin oil up to 900 bar to ensure that there were no leakages within the flowlines. The DMA HPM density measuring cell was also calibrated using paraffin oil at different temperature and pressure conditions. Additional calibrations were conducted using the original oil-based drilling fluid to ensure the repeatability of density measurements at 150 °C and 100 bar.

2.6 Herschel–Bulkley rheological parameters

The three-parameter Herschel–Bulkley (H-B) model was used to describe the flow characteristics of the fluid sample. This is the most accepted model by the oil and gas industry for drilling fluids. The general definition of the H-B model is expressed as a function of the power-law model and a yield stress term as follows [19]:

$$\tau(\dot{\gamma}) = \tau_{yFC} + K\dot{\gamma}^n. \quad (2)$$

Here, n , is the flow behavior index, K , is the consistency index, and τ_{yFC} , is the yield stress. Parameters of n and K can be determined by a least-square regression of the flow curve data after the yield stress τ_{yFC} , is quantified. The yield stress is estimated by extrapolation from the low shear rate down to zero-shear rate. The yield stress in this work is approximated as:

$$\tau_{yFC} = \tau_1 - \dot{\gamma}_1 \left(\frac{\tau_2 - \tau_1}{\dot{\gamma}_2 - \dot{\gamma}_1} \right). \quad (3)$$

From Eq. (3), the yield stress value can be extrapolated linearly from the two lowest shear rates of a flow curve at 3 and 6 rpm from a Fann viscometer reading. A similar approach was proposed by Power and Zamora [36].

It should be noted that the yield stress value computed from Eq. (3) could either be higher or lower than the actual yield stress depending on the drilling fluid composition. However, the extrapolated yield stress values are reasonable

Table 2 Physical components and functions of the experimental setup

Name of item	Function of item
DMA HPM density measuring cell	Density measuring cell for HPHT for pressures up to 1400 bar and temperature up to 200 °C. Density range from 0 to 3 g/cm ³ . Sample in the measuring cell ~ 2 mL
Waste cylinder	Stores waste fluids from the mixing and gas cylinders. It also provides backpressure to the density measuring cell through pump B
Mixing cylinder	Charged with the test fluid sample. It also encased in a controlled heating jacket with temperature up to 200 °C
Gas cylinder	Charged with N ₂ gas to be introduced into the mixing cylinder
Rheometer (MCR 102)	Characterizes the rheological properties of the fluid sample. It is also fitted with a pressure cell for HPHT conditions
Syringe pumps	Provides continuous constant flow or pressure. Each piston cylinder has a capacity of 68 mL. The flow range is up to 25 mL/min and pressure range is up to 1379 bar

for most drilling fluids as long as the standard viscometer instruments are used.

It could be observed from the classical H-B model representation that the consistency index, K , is dependent dimensionally on the flow behavior index, n . This representation is not well suited for optimal digitalization process of hydraulic systems in the drilling industry. To alleviate this anomaly, Saasen and Ytrehus introduced a dimensionless shear rate where a characteristic shear rate is selected for the flow. This representation of the H-B model is given as follows [42, 43]:

$$\tau(\dot{\gamma}) = \tau_{yFC} + \tau_{ss} \left(\frac{\dot{\gamma}}{\dot{\gamma}_s} \right)^n \tag{4}$$

Here, the surplus shear stress is expressed as $\tau_{ss} = \tau(\dot{\gamma}_s) - \tau_{yFC}$. The shear stress, $\tau(\dot{\gamma}_s)$, is measured at a predefined shear rate, $\dot{\gamma}_s$, which is dependent of the flow process to be analyzed. The flow behavior index, n , can be quantified from the expression given as:

$$n = \ln \left(\frac{\tau_x - \tau_{yFC}}{\tau_{ss}} \right) / \ln \left(\frac{\dot{\gamma}_x}{\dot{\gamma}_s} \right), \tag{5}$$

where the shear rate, $\dot{\gamma}_x$, and $\dot{\gamma}_s$, should be within the relevant range for the flow problem to be evaluated, and τ_x is the shear stress measured at $\dot{\gamma}_x$. In this analysis, the following shear rate values are used, $\dot{\gamma}_x = 100\text{s}^{-1}$ and $\dot{\gamma}_s = 300\text{s}^{-1}$. The consistency index, K , can be expressed as:

$$K = \frac{\tau_{ss}}{\dot{\gamma}_s^n} \tag{6}$$

In cases where the flow is very slow and the numerical value of the shear rate is close to or less than unity, a comparison between different fluids' consistency indexes would be meaningful. This is because at a shear rate of one, the shear stress will then be numerically equal to the sum of the yield stress and the consistency index as long as consistent dimension units are used.

3 Results and analyses

3.1 Flow curves analyses at atmospheric and HPHT conditions

We compared the flow curves measurements between batch 1 and batch 2 at 20 °C and 90 °C at atmospheric pressure condition as presented in Fig. 3. It is observed that batch 1 and batch 2 flow curves measurements are in good agreement within the applied shear rates at each operating condition. An exact match is not expected, both because of the different viscosities of the base fluids and also because different mixers were used when mixing the fluids. The latter

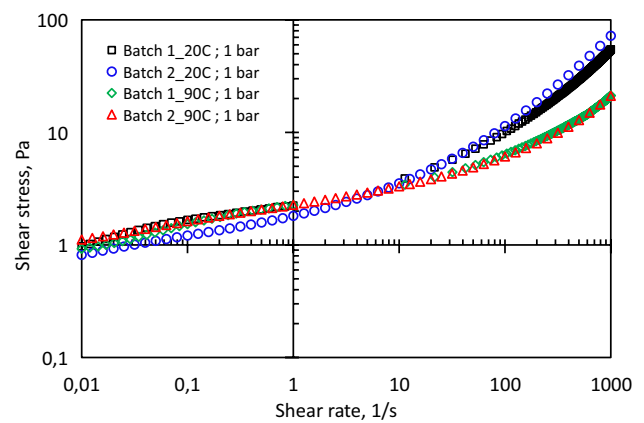


Fig. 3 Comparison of flow profile measurements between batch 1 and batch 2 at 20 °C and 90 °C at atmospheric pressure condition. Batch 1 and batch 2 contain the chemicals EDC 95/11 and ESCAID 120 ULA as base mineral oil, respectively

is expected to affect the droplet size distribution. For subsequent analysis, only data from batches 2 and 2B (i.e. with and without barite particles) would be presented.

We define a Peclet number which compares the timescale of diffusion of particle and the timescale of the flow as:

$$Pe = \frac{t_d}{t_h} = \frac{6\pi\mu a^3 \dot{\gamma}}{k_B T}, \tag{7}$$

where a is size of particle, μ is filtrate viscosity, k_B is Boltzmann constant, and T is temperature.

If the Peclet number is low, this means that the particle diffuses so fast that they have the time to build a microstructure (stop of the flow) or to form big aggregate (increase of viscosity) due to their attractive interaction. If the Peclet number is high, then flow is fast enough to prevent any formation of microstructure or aggregate which can stop the flow or make the flow more difficult (increase of viscosity). We thus observe that the definition of such a number allow us to define two regimes of flow of Brownian suspensions which are separated by a critical shear rate, which is a function of temperature and viscosity of the suspending medium [4].

An alternative way of using the Peclet number definition could be to fix the shear rate and plot the Peclet number versus temperature. The Peclet number depends on temperature both directly and through the continuous phase viscosity. Both factors tend to reduce the Peclet number with increasing temperature, thus increasing the significance of Brownian motion over hydrodynamic forces and consequently increasing the ability of the particles to build microstructure and overall viscosity.

Figure 4 shows the flow curves data measured at atmospheric pressure and atmospheric and high temperature

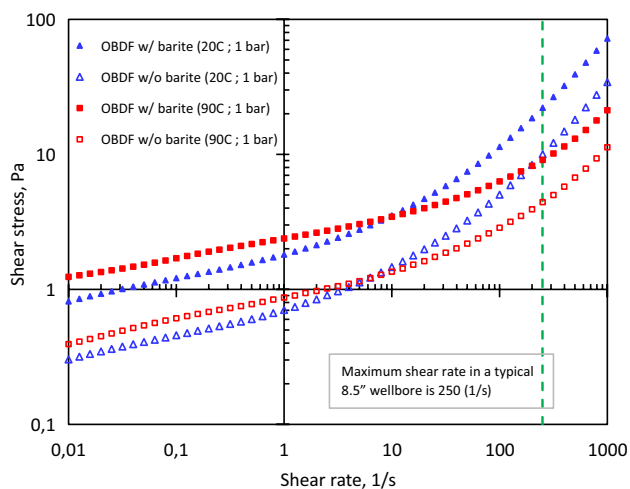


Fig. 4 Shear stress versus shear rate relationship showing the dependency of flow curves on the presence of barite particles and temperature

conditions. Here, we included data for fluid samples with and without barite particles. The flow profiles describe a pseudoplastic shear-thinning behavior at all shear rates with fluid samples having barite particles showing less shear-thinning effect than fluid samples without barite particles. The temperature effect on the viscosity is more pronounced beyond 10 s^{-1} at atmospheric pressure condition, however, temperature has less effect on the viscosity of the fluid sample with barite particles compared to fluid sample without barite. We also observed that in the low shear region (below 10 s^{-1}), the increase in temperature resulted in an increase in the fluid viscosity, both with and without barite particles. This can be explained by Brownian motion as discussed above, but heat activation of the viscosifiers could also contribute to this viscosity increase. Both effects would contribute to lower barite sag and better suspension of the particles. The effect of the viscosifiers is diminished at high shear rates, hence the drastic decrease in the fluid samples viscosity as the temperature increased. It is also observed that the yield stress of the fluid samples increased with increasing temperature at atmospheric pressure condition.

Figure 5 also shows the effect of high pressure and high temperature on the fluid samples. Measurements at 1 bar are presented for reference. It should also be noted that all measurements conducted in Fig. 5 were conducted using the pressure cell and only shear rates data from 10 s^{-1} and above are reported. This is because in the low shear rate region below 10 s^{-1} , the measurements were erratic. This was believed to be due to higher intrinsic friction of the pressure cell in the low shear region. For the measurements with barite particles, the measurements could possibly also be affected by particles trapped in the bearings of the pressure cell. This was later evidenced by observing traces of barite particles

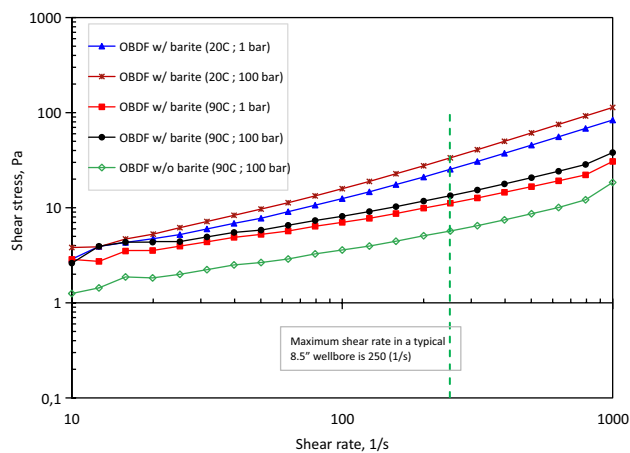


Fig. 5 Shear stress vs shear rate relationship showing the dependency of flow curves on the presence of barite particles, pressure and temperature. All measurements were conducted using the pressure cell

trapped within these bearings. Several attempts were made after cleaning the bearing, followed by motor adjustment and a precision air check, yet we could not generate accurate measured data within the low shear region. Other investigators have also reported similar technical challenges when using the pressure cell [8, 21, 49].

It is observed that at constant temperature, increasing pressure also increased the viscosity of the fluid samples, however, the increase is more pronounced in the fluid sample with barite particles. This is due to low compressibility of the barite particles. This phenomenon could promote particles suspension in high pressured wellbore, thereby minimizing barite sag. The study further revealed that the viscosity of the fluid sample is lower at HPHT condition ($90 \text{ }^\circ\text{C}$ and 100 bar) compared to atmospheric condition ($20 \text{ }^\circ\text{C}$ and 1 bar). This shows that the temperature effect dominates over the pressure effect at high shear rates.

Relevant wall shear rates as function of pipe and wellbore diameters can be found from the expression for wall shear rate of a Newtonian fluid in a concentric annulus, i.e. $12v/(D_o - D_i)$. Here v is the axial velocity and D_o and D_i are the hole size and drillpipe diameters, respectively, as shown by, for example, Guillot [19]. The wall shear rate at same flow rate is slightly larger for a shear-thinning fluid, but it is reduced again when the annulus is eccentric. When we consider a shear rate of approximately 250 s^{-1} , which is typically the maximum shear rate experienced in 8.5 inch hole annulus [45], and HPHT condition, the viscosity of the fluid sample with barite particles measured at $90 \text{ }^\circ\text{C}$ and 100 bar increased on average 20% relative to the fluid viscosity measured at $90 \text{ }^\circ\text{C}$ and 1 bar . For the fluid sample without barite particles, the viscosity measured at $90 \text{ }^\circ\text{C}$ and 100 bar decreased on average 57% relative to the fluid viscosity with barite measured at $90 \text{ }^\circ\text{C}$ and 100 bar . Figure 6 shows that

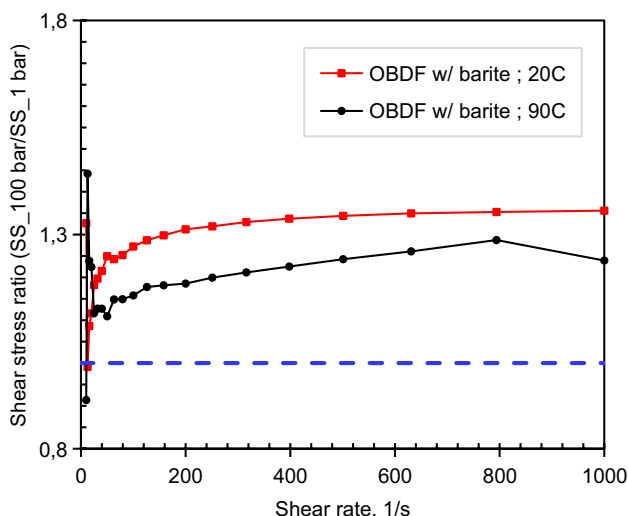


Fig. 6 Ratio of shear stress at 100 bar to shear stress at 1 bar as a function shear rate. All measurements were conducted using the pressure cell

the effect of pressure on viscosity increases with increasing shear rate both at 20 °C and 90 °C. The effect, however, is more pronounced at 20 °C.

3.2 Oscillatory sweep analyses at different temperatures and atmospheric pressure conditions

Figure 7a, b shows the amplitude sweep curves for fluid samples with and without barite particles, respectively, at 20 °C and 90 °C and atmospheric pressure condition. These curves describe the elastic and viscous moduli of the fluid samples at varying strain amplitude. The structural character of the fluid samples show that the elasticity exceeds the viscous behavior, i.e., $G' > G''$, exhibiting a gel-like character within the linear viscoelastic (LVE) range, and a liquid-like character at higher amplitudes, where the flow point, $G' = G''$ is where the elastic behavior becomes less than the viscous behavior. It is observed in

Fig. 7a that within the entire strain rate range, there is a minor difference between the elasticity values, G' , of the fluid sample measured at 20 °C and 90 °C at atmospheric pressure condition. This insignificant difference may be as a result of fluid evaporation as temperature increases. In contrast, for fluid sample without barite particles, as shown in Fig. 7b, there is a shift in the elasticity values particularly within the LVE range as the temperature increased. This could be as a result of the heat-activated viscosifiers causing the elasticity of the fluid sample to increase. It is worth noting that at a temperature of 90 °C, the presence of barite particles increased the elasticity of the fluid sample within the LVE range about 5 times that of the fluid sample without barite at.

The dynamic yield stress is here determined from amplitude sweep curves where a harmonically varying shear strain with different amplitudes is applied at a constant frequency of 10 rad^{-1} . The yield stress is then defined in terms of the end of the linear viscoelastic (LVE) region. To be specific, we define this yield stress as the shear stress where $G' = G''$, and we denote this yield stress as τ_{yOSC} . A similar approach was used by Bonn et al. [10]. Other methods for estimating the yield stress from oscillatory sweep tests have been reported by Rouyer et al. [38] and Dinkgreve et al. [14].

Practical users often prefer to use the flow point criterion ($G' = G''$) for yield stress as the basis of evaluation since they want to know the point at which the internal structure is breaking to such an extent causing the material to flow finally. It is known that there will be large uncertainties in determining the correct low shear rate as function of rotation rate in the presence of a yield stress or a low power-law index when measuring the flow curve using a concentric cylinder device [46]. Thus, it is difficult to measure the yield stress from flow curves using concentric cylinder options. Still, this method is used in industrial standard by extrapolation [7, 36]. In this paper, the flow curve approach estimates the yield stress by extrapolation from low shear rates to zero-shear rate. Therefore, it is possible that the alternative measurement of the yield stress using oscillatory rheometry at fixed frequency can be more applicable.

Fig. 7 Elastic and viscous moduli curves versus strain amplitude measured at 20 °C, 90 °C and 1 bar: **a** fluid sample with barite particle and **b** fluid sample without barite particles

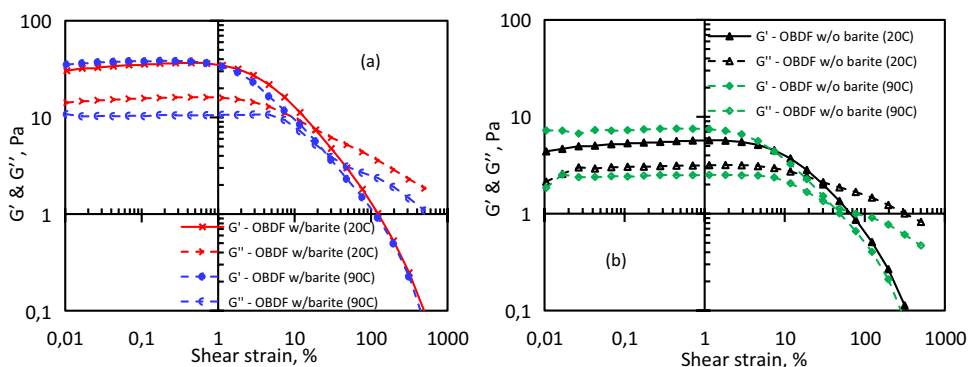


Table 3 Estimation of yield stress and shear strain from oscillatory rheometry at atmospheric pressure condition

	Fluid sample w/ barite		Fluid sample w/o barite	
	20 °C	90 °C	20 °C	90 °C
Yield stress, τ_{yOSC} , (Pa)	1.993	1.506	0.880	0.663
Yield strain, γ , (%)	18.9	22.6	30.2	37.9

Table 3 shows the estimated yield stress, τ_{yOSC} , and the corresponding yield strain values for fluid samples with and without barite particles measured at 20 °C, 90 °C and 1 bar. It is observed from Table 3 that the yield stress values of the fluid samples decrease with increasing temperature while the yield strain increase with increasing temperature. This applies to both to fluids samples with and without barite particles. On the other hand, the yield stress is significantly higher by a factor of more than two in the sample with barite at both temperatures.

Figure 8 shows the measurement of time-dependent behavior of elasticity, G' from oscillatory measurements at constant amplitude and frequency, at 25 °C and 90 °C and atmospheric pressure condition for a fluid sample with barite particles. The strain amplitude value is chosen within the LVE range where the fluid structure is stable. At 20 °C, there is initial structural growth up to 60 min, while afterward a structural breakdown is observed due to decreasing interaction forces, thus causing a separation of the barite particles in the fluid sample. This test also shows the critical time below which the fluid sample remains stable. It is evidenced that after 60 min the fluid sample becomes unstable with

respect to barite sag. Conversely, at 90 °C, the fluid sample shows a continuous structural growth over the entire time period. This indicates that the fluid is more stable and can suspend barite particles. Although below 60 min the elastic values at 90 °C are lower than at 20 °C, a dramatic increase in G' is recorded after this time period. This increase in elasticity is, however, caused by the heat-activated chemicals in the fluid sample. Note that it was not possible to conduct oscillatory rheometry measurements at high pressure (100 bar), as the rheometer torque due to internal friction in the instrument was comparable to or larger than the measurement torque in this range. This is also the reason why we were only able to measure flow curve shear stress above a shear rate of about 10 s^{-1} at a pressure of 100 bar.

3.3 Analysis of Herschel–Bulkley rheological parameters

Using the Saasen-Ytrehus [42] Herschel–Bulkley (H-B) representation with $\dot{\gamma}_x = 100 \text{ s}^{-1}$ and $\dot{\gamma}_s = 300 \text{ s}^{-1}$, the rheological parameters of the fluid sample computed at each measured condition at atmospheric pressure are presented in Table 4. It should be noted that the consistency index, K , and flow behavior index, n , values are calculated from the flow curves using Eqs. (5 and 6), after first determining the yield stress from Eq. (3). This yield stress value is here denoted as τ_{yFC} . Results in Table 4 indicate that τ_{yFC} , and K , values increase with increasing temperature for all fluid samples. However, there is a decrease in the flow behavior index, n , values as the temperature increased, thus, making the fluid samples more shear-thinning.

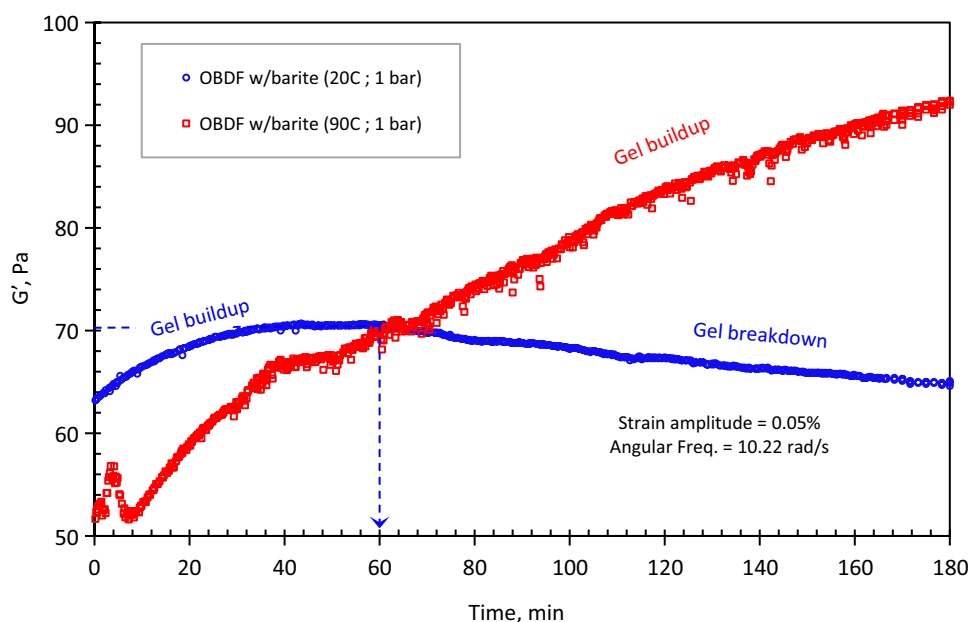
Fig. 8 Elastic modulus versus time for fluid sample measured at different temperature conditions

Table 4 H-B model parameters and significance values R^2 based on flow curve measurements at atmospheric pressure for samples with and without barite particles at 20 °C and 90 °C

Sample measuring temperature	Yield stress, τ_{yFC} (Pa)		Consistency index, K (Pa s ⁿ)		Flow behavior index, n (-)		Surplus stress, τ_{ss} (Pa)		R^2	
	w/ barite	w/o barite	w/ barite	w/o barite	w/ barite	w/o barite	w/ barite	w/o barite	w/ barite	w/o barite
20 °C	0.677	0.245	0.313	0.126	0.767	0.790	24.845	11.392	0.9872	0.9892
90 °C	1.106	0.328	0.579	0.222	0.477	0.529	8.788	4.531	0.9528	0.9600

Corresponding values of K , n and τ_{ss} are shown in corresponding columns

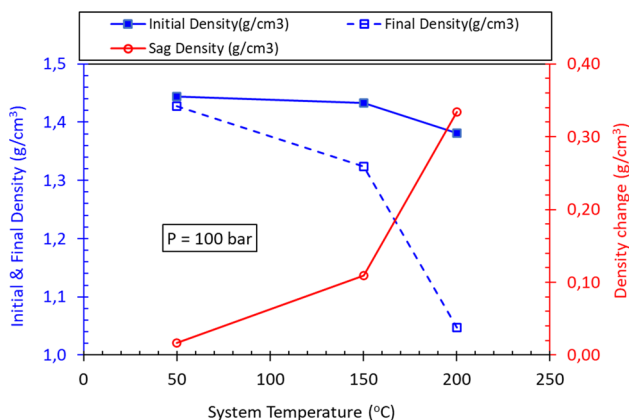


Fig. 9 Temperature dependence on initial and final fluid density at constant pressure of 100 bar

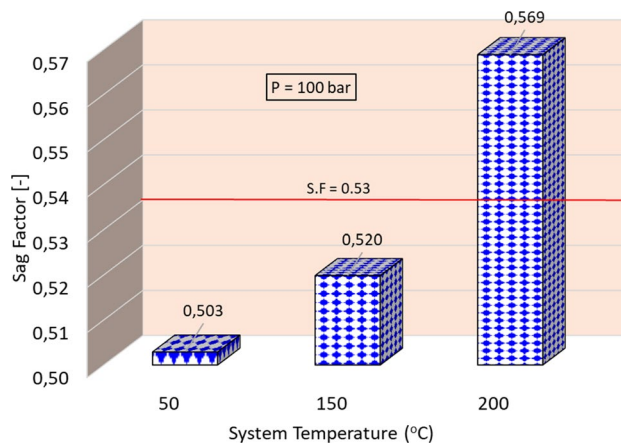


Fig. 10 Temperature dependence on barite sag factor at constant pressure of 100 bar

We also noticed that the yield stress, τ_{yOSC} , values which are estimated from oscillatory rheometry are higher than those extrapolated from the flow curves. While the flow curve method predicts an increase in yield stress with increasing temperature, a decrease in yield stress with increasing temperature is predicted from the oscillatory rheometry method.

3.4 Temperature and pressure dependency on barite sag

Barite sag was measured using the setup and procedure described in Sect. 2.5. To ensure consistency of the measurements, we repeated the first test which was conducted at 150 °C and 100 bar and compared their results. Each test took 24 h to measure the initial and final densities. The difference in sag density between the two tests was marginal with an estimate of 4.9%.

The effects of temperature and pressure on barite sag were evaluated from the density measurements. Figure 9 presents the initial density measurements for the homogenized fluid sample and the final density measurements after a static condition for 24 h at a constant pressure condition of 100 bar. The density change, also known as sag density, is the difference between the initial and final density readings.

It is observed that as the system temperature increases, the density of the fluid sample decreases with a significant drop at 200 °C, particularly for the final density measurements. This drop in initial density is as a result of thermal expansion of the fluid. It is worth noting that the sag density increased remarkably more than 20 times as the temperature increased from 50 to 200 °C. The influence of temperature on sag is further shown in Fig. 10 in terms of static sag factor as defined in Eq. (1). It is evident that for the system temperature of 200 °C the sag factor exceeded the threshold value of 0.53, above which barite particles sediment in the fluid sample, thereby creating a density gradient in the fluid column. During drilling operation, a density gradient in the wellbore could result in gas kick at the low-density column, and in the case of oil-based drilling fluid, the gas kick would initially be dissolved in the fluid system until equilibrium saturation is reached. This can lead to well control issues if it is not detected early. Furthermore, the results in Fig. 10 show that the fluid sample will promote very little to no barite sag at system temperatures of 50 °C and 150 °C.

As shown in Fig. 11, both initial and final densities of the fluid sample increased as a result of increasing pressure at a constant temperature of 150 °C. It should be noted that we can explain the density increase with

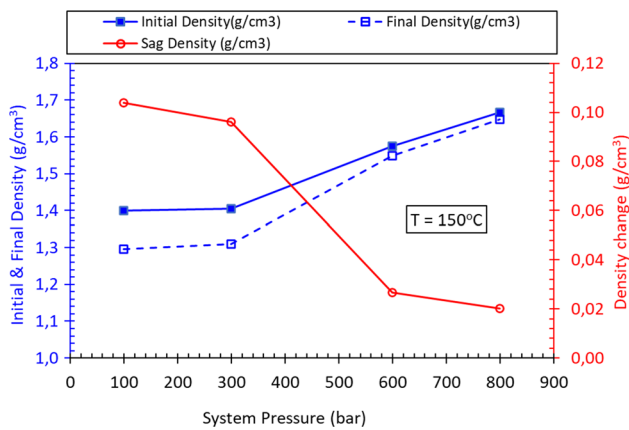


Fig. 11 Pressure dependence on initial and final fluid density at constant temperature of 150 °C

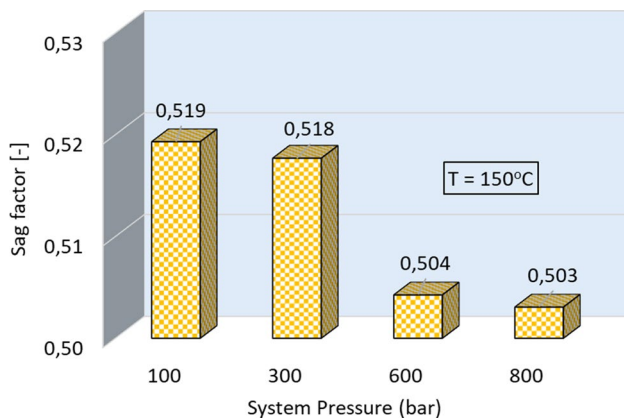


Fig. 12 Pressure dependence on barite sag factor at constant temperature of 150 °C

increasing pressure only in part by the fluid compressibility. The remaining part is not explained. However, we believe this is caused by some systemic effect which would affect both initial and final density measurements and thus not the density change. However, this remains to be verified. The density change or sag density, however, decreased at high pressure condition. This indicates that less particles tend to sediment in the fluid system at high pressures, hence the fluid sample is less prone to barite sag at high pressures. Figure 11 also reveals that the sag density recorded at 800 bar is 5 times less than that measured at 100 bar. The sag factor presented as a function of pressure at 150 °C is shown in Fig. 12. It is observed that the calculated sag factor values at all measured pressure conditions at 150 °C were below the threshold value of 0.53, indicating a favorable condition to avoid sag.

4 Discussion

Although drilling fluid properties play a key role to minimizing sag, the failure to use proper drilling practices can easily override certain drilling fluid contributions. It should be noted that even drilling fluids with ideal properties cannot fully suspend barite under all conditions.

The results obtained from this study indicate that key drilling fluid adjustments include increasing the low shear rate viscosity and improving suspension properties using rheology modifiers. We can infer that the increase in pressure and temperature could cause the elastic stiffness of the fluid to increase dramatically within the LVE range. This would create a rigid microstructure within the fluid sample which is vulnerable to break, and thus promote sag. While the rheological characterization cannot explain directly the observed increased resistance to barite sag at high pressures, we noted an increase in shear stress and thus viscosity from the flow curves at 100 bar relative to atmospheric conditions. It is reasonable to assume that this trend also extends to low shear rates and to yield stress. However, direct determination of yield stress at high pressure and high temperature (HPHT) conditions is challenging and this assumption remains to be verified.

Time dependence of the elastic modulus, G' , at 1 bar changed dramatically from 25 to 90 °C, where a strong gel buildup was seen at the higher temperature. The high temperature condition could thus increase the gel strength of the fluid sample which is necessary for static suspension, however, high pumping rate is required to restart flow circulation. On the other hand, high temperature could have negative impact on the dynamic yield stress of the drilling fluid sample which could result in a low particle suspension within the fluid sample. Excessive thinning and flocculation of the drilling fluid, which create free water and reduce low shear rate viscosities, should be avoided. Furthermore, incorrect barite wetting in non-aqueous drilling fluids would promote hard setting, and thus, intensify sag potential. To mitigate barite sag particularly in critical sections of the wellbore, between 40° and 60° hole angle, it is important to increase the annular velocity to provide energy to minimize bed deposition and also remove existing beds. Drill pipe rotation and reciprocation are also necessary to enhance the benefits of high annular velocity.

We also found that temperature has less effect on the viscosity of the fluid sample with barite particles compared to the fluid sample without barite. This can be explained that without barite particles all the fluid parts are influenced by temperature and pressure. When barite is added, only the particle sizes affected by Brownian motion (less than around 5 micron) will be influenced by temperature effect. For the larger particle sizes, being the majority

of barite particles in the fluid, the particles are expected to contribute more or less equally to the viscosity.

5 Conclusion

We have evaluated the effects of HPHT conditions on the rheological properties and barite sag potential in oil-based drilling fluid. The barite sag in a static condition was characterized using a new HPHT test cell whereas the rheological properties were measured using a rotational rheometer under atmospheric and downhole conditions.

The following conclusions can be stated from the obtained results.

1. The viscosity of the fluid sample decreased with increasing temperature at high shear rates, while an increase in viscosity was observed with increasing temperature in the low shear region.
2. The temperature effect on viscosity dominates at high shear rates compared to pressure effect.
3. The yield stress values predicted from oscillatory rheometry are generally higher than the yield stress values extrapolated from the flow curves.
4. Rheological characterization indicates a complex dependence of particle suspension and thus of barite sag on temperature, as flow curve measurements indicate increasing yield stress with temperature, while oscillatory rheometry measurements indicate decreasing yield stress with increasing temperature.
5. The sag density at 100 bar increased more than 20 times as temperature increased from 50 to 200 °C, indicating a significant rise in barite sag.
6. Increasing pressure from 100 to 800 bar at 150 °C resulted in more than 5 times reduction in the sag density, thus minimizing barite sag.

Acknowledgements We acknowledge the permission granted by both NTNU and SINTEF in Norway to use their laboratories to conduct our experiments. We further acknowledge the financial support given by the Research Council of Norway and the National Science Foundation of USA under Award Number 1743794 for the PIRE project "Multi-scale, Multi-phase Phenomena in Complex Fluids for the Energy Industries". Special appreciation goes to M-I SWACO, Schlumberger Norge AS and Anton Paar, Norway for providing technical support for our research.

Funding Open access funding provided by SINTEF.

Data availability Data supporting the results of the study will be made available subject to an internal approval process.

Open Access This article is licensed under a Creative Commons Attribution 4.0 International License, which permits use, sharing, adaptation, distribution and reproduction in any medium or format, as long as you give appropriate credit to the original author(s) and the source, provide a link to the Creative Commons licence, and indicate if changes

were made. The images or other third party material in this article are included in the article's Creative Commons licence, unless indicated otherwise in a credit line to the material. If material is not included in the article's Creative Commons licence and your intended use is not permitted by statutory regulation or exceeds the permitted use, you will need to obtain permission directly from the copyright holder. To view a copy of this licence, visit <http://creativecommons.org/licenses/by/4.0/>.

References

1. Ackerson BJ (1990) Shear induced order and shear processing of model hard sphere suspensions. *J Rheol* 34:553–590
2. Al-Bagoury M, Steele C (2012) A new, alternative weighting material for drilling fluids. In: Presented at the IADC/SPE drilling conference and exhibition, San Diego, California, USA, 6–8 March. SPE 151331-MS <https://doi.org/10.2118/151331-MS>
3. Amani M, Al-Jubouri M, Shadravan A (2012) Comparative study of using oil-based mud versus water-based mud in HPHT fields. *Adv Petrol Explor Dev* 4(2):18–27. <https://doi.org/10.3968/j.aped.1925543820120402.987>
4. Ansari M, Turney DE, Morris J, Banerjee S (2021) Investigations of rheology and a link to microstructure of oil-based drilling fluids. *J Petrol Sci Eng*. <https://doi.org/10.1016/j.petrol.2020.108031>
5. Atolini TM, Ribeiro PR (2007) Vapour-liquid mixture behavior at high temperatures and pressures: a review directed to drilling engineering. *Braz J Petrol Gas* 1(2):123–130
6. API 13A (2004) Specification for drilling-fluid materials, sixteenth edition and ISO 13500:1998 (modified) petroleum and natural gas industries - drilling fluid materials-specification and tests
7. API 13B-1 (2003) Recommended practice for field testing water-based drilling fluids, 3rd ed
8. Arnolds O (2013) Rheology at high pressure—setup and performance of the 1000 bar pressure cell. *Anton Paar Application Report*
9. Bol GM, Wong S-W, Davidson CJ, Woodland DC (1994) Borehole stability in shales. *SPE Drill Complet* 9(2):87–94. <https://doi.org/10.2118/24975-PA>
10. Bonn D, Denn MM, Berthier L, Divoux T, Manneville S (2017) Yield stress materials in soft condensed matter. *Rev Mod Phys* 89(3):035005
11. Borges RFO, De Souza RSVA, Vargas MLV, Scheid CM, Caçada LA, Meleiro LAC (2022) Analysis of the stability of oil-based drilling muds by electrical stability measurements as a function of oil-water ratio, weighting material and lubricant concentrations. *J Petrol Sci Eng* 218:110924
12. Boycott AE (1920) Sedimentation of blood corpuscles. *Nature* 104:532
13. Cayeux E (2020) Time, pressure and temperature dependent rheological properties of drilling fluids and their automatic measurements. In: Presented at the IADC/SPE international drilling conference and exhibition, Galveston, Texas, USA, 3–5 March. SPE 199641-MS <https://doi.org/10.2118/199641-MS>
14. Dinkgreve M, Paredes J, Denn MM, Bonn D (2001) On different ways of measuring “the” yield stress. *J Nonnewton Fluid Mech* 238:233–241
15. Dye W, Hemphill T, Gusler W, Mullen G (2001) Correlation of ultralow-shear-rate viscosity and dynamic barite sag. *SPE Drill Complet* 16:27–34
16. Ehrhorn C, Saasen A (1996) Barite sag in drilling fluids. *Ann Trans Nordic Rheol Soc* 4:66–68
17. Elkhatny S (2019) Mitigation of barite sagging during the drilling of high-pressure high-temperature wells using an invert emulsion

- drilling fluid. *Powder Technol* 352:325–330. <https://doi.org/10.1016/j.powtec.2019.04.037>
18. Flatabø GØ, Torsvik A, Oltedal VM, Bjørkvik B, Grimstad A-A, Linga H (2015) Experimental gas absorption in petroleum fluids at HPHT conditions. In: Presented at the SPE Bergen one day seminar, Bergen, Norway, 22 April. SPE-173865-MS <https://doi.org/10.2118/173865-MS>
 19. Guillot D (1990) Digest of rheological equations. In: Nelson EB (ed) *Well cementing*. Elsevier, Amsterdam
 20. Herschel WH, Bulkley R (1926) Konsistenz-messungen von Gum-mibenzöllösungen. *Kolloid Z* 39:291–300
 21. Heyer P (2014) Guideline for the pressure cell. *Anton Paar Application Report*.
 22. Jachnik R (2005) Drilling fluid thixotropy & relevance. *Ann Trans Nordic Rheol Soc* 13:1–6
 23. Jamison DE, Clements WR (1990) A new test method to characterize setting/sag tendencies of drilling fluids used in extended reach drilling. *ASME Drill Technol Symp* 27:109–113
 24. Kulkarni SD, Savari S, Murphy R, Hemphill T, Jamison DE (2014) "Improved" barite sag analysis for better drilling fluid planning in extreme drilling environments. In: AADE fluids technical conference and exhibition, Hilton Houston North Hotel, Houston, 15 & 16 April.
 25. Massam J, Popplestone A, Burn A (2004) A unique technical solution to barite sag in drilling fluids. In: Paper AADE-04-DF-HO-21. AADE 2004 drilling fluids conference. The Radisson Astrodome, Houston, 6–7 April.
 26. Maxey J (2007) Rheological analysis of static and dynamic sag in drilling fluids. *Annu Trans Nordic Rheol Soc* 15:181–188
 27. Mitchell J (2019) Magnetic resonance diffusion measurements of droplet size in drilling fluid emulsions on a benchtop instrument. *Colloids Surf A* 564:69–77. <https://doi.org/10.1016/j.colsurfa.2018.12.033>
 28. Movahedi H, Shad S, Mokhtari-Hosseini ZB (2018) Modeling and simulation of barite deposition in an annulus space of a well using CFD. *J Petrol Sci Eng* 161:476–496. <https://doi.org/10.1016/j.petrol.2017.12.014>
 29. Nguyen TC, Miska S, Saasen A, Maxey J (2014) Using Taguchi and ANOVA methods to study the combined effects of drilling parameters on dynamic barite sag. *J Petrol Sci Eng* 121:126–133
 30. Nguyen T, Miska S, Yu M, Takach N, Ahmed R, Saasen A, Omland TH, Maxey J (2011) Experimental study of dynamic barite sag in oil-based drilling fluids using a modified rotational viscometer and a flow loop. *J Petrol Sci Eng* 78:160–165
 31. Ofei TN, Kalaga DV, Lund B, Saasen A, Linga H, Sangesland S, Gyland KR, Kawaji M (2020) Laboratory evaluation of static and dynamic sag in oil-based drilling fluids. *SPE J*. <https://doi.org/10.2118/199567-PA>
 32. Ofei TN, Itung C, Lund B, Saasen A, Sangesland S (2020) On the stability of oil-based drilling fluid: effect of oil-water ratio. In: Proceedings of the ASME 2020 39th international conference on ocean, offshore and arctic engineering. 11, *Petroleum Technology* <https://doi.org/10.1115/OMAE2020-19071>
 33. Ofei TN, Lund B, Saasen A, Sangesland S, Gyland KR, Linga H (2019) A new approach to dynamic barite sag analysis on typical field oil-based drilling fluid. *Annu Trans Nordic Rheol Soc* 27:61–69
 34. Omland TH (2009) Particle settling in non-Newtonian drilling fluids. PhD Thesis UiS no. 80, University of Stavanger.
 35. Omland TH, Saasen A, Amundsen PA (2007) Detection techniques determining weighting material sag in drilling fluid and relationship to rheology. *Annu Trans Nordic Rheol Soc* 15:1–9
 36. Pähz T, Durán O, de Klerk DN, Govender I, Trulsson M (2019) Local rheology relation with variable yield stress ratio across dry, wet, dense, and dilute granular flows. *Phys Rev Lett* 123(4):048001
 37. Parvizinia A, Ahmed RM, Osisanya SO (2011) Experimental study on the phenomenon of barite sag. In: Presented at the international petroleum technology conference, Bangkok, Thailand, 15–17 November. IPTC-14944-MS. <https://doi.org/10.2523/IPTC-14944-MS>
 38. Power D, Zamora M (2002) Drilling fluid yield stress: measurement techniques for improved understanding of critical drilling fluid parameters. In: Paper AADE-03-NTCE-35 the AADE 2003 National Technology Conference., Houston.
 39. Rocha RR, Oechsler BF, Meleiro LAC, Fagundes FM, Arouca FO, Damasceno JJR, Scheid CM, Calçada LA (2020) Settling of weight agents in non-Newtonian fluids to off-shore drilling wells: modeling, parameter estimation and analysis of constitutive equations. *J Petrol Sci Eng* 184:106535. <https://doi.org/10.1016/j.petrol.2019.106535>
 40. Rouyer F, Cohen-Addad S, Hohler R (2005) Is the yield stress of aqueous foam a well-defined quantity? *Colloid Surf A* 263:111–116
 41. Saasen A (2002) Sag of weight materials in oil-based drilling fluids. In: Paper presented at the IADC/SPE Asia Pacific Drilling Technology, Jakarta, Indonesia. 09 September. SPE-77190-MS <https://doi.org/10.2118/77190-MS>
 42. Saasen A, Hodne H (2016) The influence of vibrations on drilling fluid rheological properties and the consequence for solids control. *Appl Rheol*. <https://doi.org/10.3933/ApplRheol-26-25349>
 43. Saasen A, Liu D, Marken CD et al (1995) Prediction of barite sag potential of drilling fluids from rheological measurements. In: Presented at the SPE/IADC drilling conference, Amsterdam, 28 February–2 March. SPE 29410-MS. <https://doi.org/10.2118/29410-MS>
 44. Saasen A, Ytrehus JD (2018) Rheological properties of drilling fluids—use of dimensionless shear rates in Herschel–Bulkley models and power-law models. *Appl Rheol* 28(5):54515. <https://doi.org/10.3933/ApplRheol-28-54515>
 45. Saasen A, Ytrehus JD (2020) Viscosity models for drilling fluids—Herschel–Bulkley parameters and their use. *Energies* 13(20):5271. <https://doi.org/10.3390/en13205271>
 46. Savari S, Kulkarni SD, Maxey J, Teke K (2013) A comprehensive approach to barite sag analysis on field muds. In: AADE national technical conference and exhibition, Cox Convention Centre, Oklahoma City, February 26–27.
 47. Sayindla S, Lund B, Ytrehus JD, Saasen A (2017) Hole-cleaning performance comparison of oil-based and water-based drilling fluids. *J Petrol Sci Eng* 159:49–57. <https://doi.org/10.1016/j.petrol.2017.08.069>
 48. Skadsem HJ, Saasen A (2019) Concentric cylinder viscometer flows of Herschel–Bulkley fluids. *Appl Rheol* 29:173–181. <https://doi.org/10.1515/arh-2019-0015>
 49. Skalle P, Backe KR, Lyomov SK, Sveen J (1999) Barite segregation in inclined boreholes. *J Can Pet Technol* 38:13
 50. Tehrani A, Zamora M, Power D (2004) Role of rheology in barite sag in SBM and OBM. In: Presented at the AADE drilling fluids conference, Houston Texas, 6–7 April
 51. Torsvik A, Myrseth V, Linga H (2015) Drilling fluid rheology at challenging drilling conditions—an experimental study using a 1000 bar pressure cell. *Annu Trans Nordic Rheol Soc* 23:45–51
 52. Wang J, Zhang J, Yan L, Cheng R, Ni X, Yang H (2021) Prevent barite static sag of oil-based completion fluid in ultra-deep wells. In: Paper presented at the international petroleum technology conference, virtual
 53. Zamora M, Jefferson D (1994) Controlling barite sag can reduce drilling problems. *Oil Gas J* 92(7):47–52

Publisher's Note Springer Nature remains neutral with regard to jurisdictional claims in published maps and institutional affiliations.